

1 Physical Basis of Prediction Methods

The large-scale magnetic field of the Sun is the result of dynamo action occurring in the solar interior. That dynamo action is in principle possible has been established by both mean-field dynamo theory (see e.g. Krause & Raedler (1980)) as well as by global three-dimensional MHD simulations (see the recent review by Charbonneau (2014)). In order to make predictions we need to understand which mechanisms and processes are responsible for producing the magnetic field actually seen on the Sun, and addressing this question requires a consideration of the observations. Section 1.1 will therefore set out the most critical observations of the Sun's magnetic field, and Section ?? the most important observations concerning the flows which produce the large-scale magnetic field. Sections ?? and ?? will then show us how the observations provide sufficient constraints to allow meaningful predictions.

1.1 Magnetic field observations

Synoptic full-disk line-of-sight magnetograms with a daily cadence (weather allowing) are available for the last four solar cycles. This is an incredibly useful resource for understanding the solar dynamo. From the synoptic full-disk magnetograms it is possible to make magnetic butterfly maps of the Sun's poloidal and toroidal (Duvall et al. (1979); Ulrich & Boyden (2005)) magnetic field at the solar surface. The Hovmöller diagrams in Figure 1 show the observed surface poloidal and toroidal magnetic fields derived from synoptic full-disk magnetograms as presented in Cameron et al. (2018).

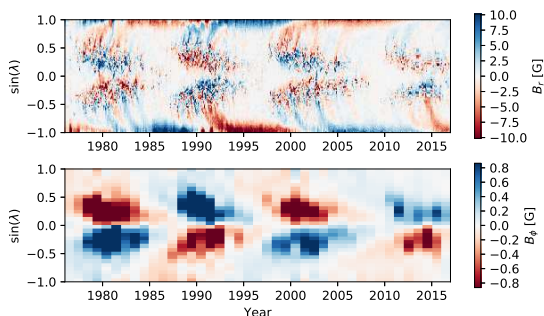


Fig. 1. Latitudinally averaged surface radial magnetic field (upper panel) and toroidal field (lower panel) as a function of latitude and time. The radial map is based on KPNSO/SOLIS full synoptic magnetograms, and the toroidal field is based on WSO synoptic observations, processed as discussed in Cameron et al. (2018).

If we want to apply flux transport models to describe the migration of actual flux towards the poles, we should model the flux at higher spatial resolution than longitudinal averages. The transport happens in several narrow 'streaks' (not broad unipolar 'surges') and both polarities migrate together (Topka et al. (1980)) generally side-by-side, as is evident when shown with higher spatial resolution than rotational zonal averages, Figure 2. In any case, the synoptic magnetograms form the basis for understanding the time evolution of solar magnetism and prediction of the solar cycle. *See also the Comment section at the end of this draft.*

Going back further in time we have regular white light photographs (see for example Howard et al. (1984) and drawings of sunspots (e.g. Leussu et al. (2017)), sunspot numbers (Clette

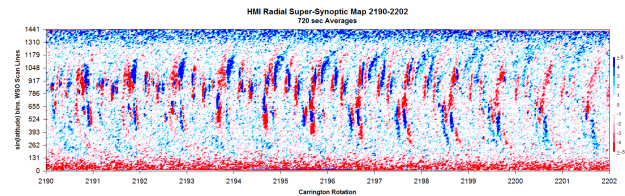


Fig. 2. Super-Synoptic Maps for the past year from HMI. The intervals on the ordinate axis show the borders of the eleven scan lines for the WSO magnetograph. Blue color: fields pointing away from the Sun (positive); red color: towards the Sun (negative). Spatial resolution is 10×1 heliographic degrees at disk center.

et al. (2014)), indices of geomagnetic fluctuations (Lockwood et al. (2014); Svalgaard (2014)) and cosmogenic nucleotides (Steinhilber et al. (2012)).

2 Polar Magnetic Field Observations

2.1 WSO Observations (Svalgaard)

There are basically three ways to assess the polar fields and their evolution: direct measurements, flux transport forwards modeling, and inferences from proxies. Direct measurements are difficult because we are directly observing only the projection of the field onto the line of sight. Measurement of the full field vector relies on theoretical inversion codes that do not work well near the limb. Various lines of evidence (e.g. Shiota (2018)) strongly suggest that the bulk of the polar fields (as everywhere on the sun) consists of sub-arc-second concentrations of strong radial magnetic fields (of kiloGauss strength). Since the field is not spatially resolved, what we are really observing is the net magnetic **flux** over the observation pixel, projected onto the line of sight, causing a dilution of the signal by a factor of the order of a thousand. Various instrumental effects, such as saturation of the magnetic signal at high field strength, and differing pixel sizes between instruments make the values reported by the observers disagree.

There is no consensus about what the 'real' true flux or field values are, with each observer team claiming that *their* measurements are the 'ground truth' and the most reliable. The best we can do then, is to **normalize** all observers to a common arbitrary base (for example, the HMI-instrument on SDO - being the 'newest' data set) based on time-overlapping data series. Figure 3 shows the result of such a normalization using data from MWO (Mount Wilson Observatory), WSO (Wilcox Solar Observatory), MDI (Michelson Doppler Imager on SOHO), and HMI (Helioseismic and Magnetic Imager on SDO).

Because of the good agreement between the (scaled) series from all the magnetographs it seems permissible to compute a straight average of their data and use the result as a canonical 'polar field' series (given in Appendix 1). Polar field values (and the dipole moment derived from them) computed from Flux transport models and proxies should reproduce these composite averages. The variation of the Dipole Moment (to the power of 0.8 as the relation is weakly non-linear) through a 'polar field' cycle from solar maximum to the next solar maximum where each value is divided by the size of that next solar cycle seems to be invariant, Figure 4, and can thus be used as a predictor of the size of that cycle, as that value which maintains the invariance. For several years before each solar minimum, the ratio so computed seems to reach a plateau (dashed line) of little variation (see also Iijima et al. (2017)). Scattered light has the effect of diminishing the

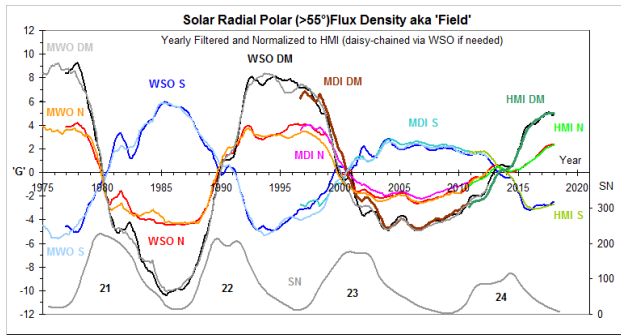


Fig. 3. A composite of the polar field measurements by the four magnetographs shown with the color coding on the Figure. All were computed from synoptic maps as the 1-year boxcar average field polewards of 55° latitude normalized to the scale of HMI. The ‘dipole moment’ DM is defined as the field in the northern polar cap minus the field in the southern.

field values and thus depressing DM during several years before efforts were made in 1978 to reduce the scattered light. With the DM-value up to the time of writing, a size of the Cycle 25 of 120 ± 10 seems to maintain the plateau. Assumed values for DM of 90 (weaker cycle, blue curve) and 160 (stronger cycle, pink curve) do not maintain the plateau. Should the coming year show us a higher (or lower) DM, the prediction would have to be adjusted accordingly.

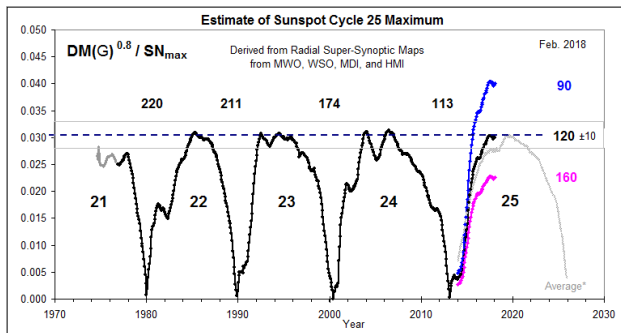


Fig. 4. The variation of the Dipole Moment (to the power of 0.8) through a ‘polar field’ cycle from solar maximum to the next solar maximum where each value is divided by the size of that next solar cycle (shown above the dashed line) seems to be invariant (see text for cycle 21) and can thus be used as a predictor of the size of that cycle, as that value which maintains the invariance (see text for prediction).

We argued (Svalgaard et al. (2005)) that once the directly observed line-of-sight WSO polar fields became stable (approximately 3 years before solar minimum) resulting in a regular annual variation, the Dipole Moment at that time could be used for prediction. At the time of writing, a regular annual variation seems to have been again established (Figure 5) with a DM value of some $135 \mu\text{T}$ versus $119 \mu\text{T}$ (1.35 G versus 1.19 G for the Tesla-challenged) prior to the previous minimum, suggesting a Cycle 25 maximum smoothed sunspot number of 128.

If we can forecast the sunspot number (SN) and the group number (GN) using DM as a predictor, then we should be able to *hindcast* the dipole moment from the SN and/or the GN. An early attempt (Jiang et al. (2011)) was partly based on the now obsolete Hoyt & Schatten Group Sunspot Numbers. We shall here use the revised activity series. As many cycles [even if smoothed] have two or more ‘peaks we use the average SN or GN for the two most active [unsmoothed] yearly values as a measure of the cycle ac-

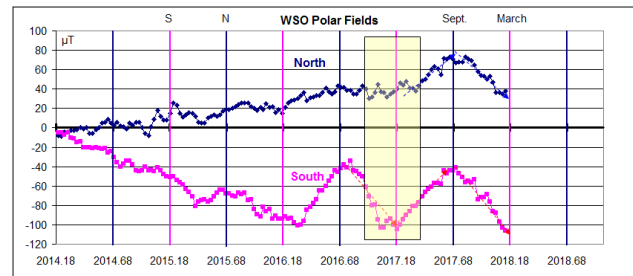


Fig. 5. The variation of the WSO polar fields since the latest reversal. The yellow rectangle shows where the magnetograph Littrow lens was contaminated (reducing the signal; this has now been corrected and the corrected values are plotted here). Times of maximum apparent tilt of the solar axis are indicated by blue and pink vertical lines.

tivity following the minima. We have four measurements of [the three-year] DM at minima at WSO since the middle of 1976. The relationships between DM μT and SN ($DM = 0.63SN^{1.12}$) and GN ($DM = 7GN^{1.52}$) are assumed to be physical rather than spurious, and are at least within the domains of observed values, plausibly extended slightly at both ends.

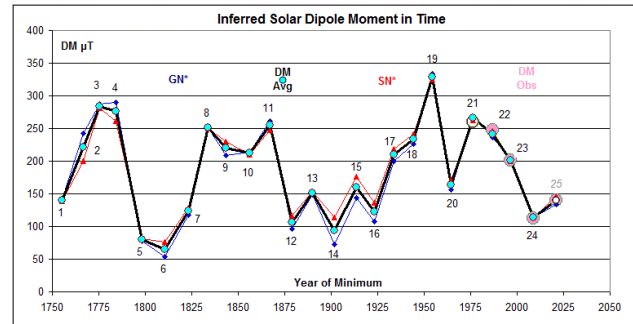


Fig. 6. The WSO solar Dipole Moment DM inferred from the sunspot number, SN (red symbols), and from the group number, GN (blue symbols) for the cycles following the minima. The average DM for each cycle is shown with a heavy black line with light-blue circles. The observed DM values since Cycle 21 are shown with large circles. An educated guess for Cycle 25 (size between Cycles 20 and 24, based on extrapolated DM from WSO) completes the inferences.

The inferred DM values can be used as basis for speculations about the long-term evolution of solar activity. An example is the variation of the heliospheric magnetic field (HMF) strength (at Earth), B , which has been derived from geomagnetic data back to at least the 1840s (Owens et al. (2016)). It is often believed that the polar fields control the HMF when the low-latitude magnetic fields from active regions have died (or migrated) away at solar minimum. We can test this assertion by plotting B at minimum against DM (Figure 7). The excess of B above a ‘floor’ of 3.9 nT does seem to be proportional to DM, leaving open the question of where the ‘floor’ comes from.

2.2 WSO Mapping to HMI

If we accept (or believe) that we can predict the size of the next solar cycle from the polar fields, an obvious way to obtain a prediction earlier is to try and predict the polar fields from modeling the poleward migration of magnetic flux from the sunspot zones. For this we should use the latest data (i.e. HMI, Hinode, and eventually SOLIS) with earlier data from MDI, WSO, and MWO (and

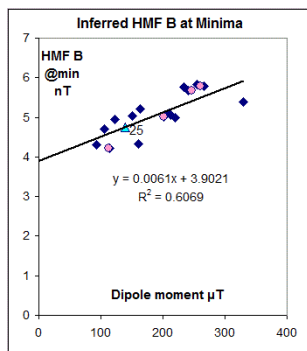


Fig. 7. HMF (Heliospheric Magnetic Field) strength at Earth inferred from geomagnetic data at sunspot minima vs. the WSO solar Dipole Moment DM for the minima from SN and GN (blue diamonds, cycles 9-24). B(DM) observed at minima before Cycles 21-24 are shown as pink circles and estimated for Cycle 25 as a green triangle.

proxies) providing supporting information and historical context.

For reasons of remapping onto heliographic coordinates, the magnetic field is assumed to be radial and the observed line-of-sight field is converted to a radial field, which also removes the arbitrary location of the observer from the equation. As WSO saturates for kiloGauss field strengths (Svalgaard et al. (1978)) we apply a saturation correction of a factor 1.8 to all WSO field values. As the hemispheric area above 55° latitude that contributes to the synoptic maps occupies only a single pixel of actual measurements by WSO, the WSO ‘polar fields’ are simply the averages of all pixels [the one and only WSO pixel corresponds to about 130,000 pixels for HMI] above 55° latitudes as a function of time (longitude).

When comparing field [actually net flux!] measurements from two instruments there is yet another factor to consider, namely the cancellation of non-resolved opposite polarities within the aperture of the instrument. The larger the aperture, the larger is the effect of cancellation, in particular at the sunspot-latitudes where there is a lot of mixed (‘salt and pepper’) polarities. The WSO magnetograph has 11 (eleven!) boustrophedonic scan lines (each 175 arc-seconds wide) from north to south. To estimate the ‘cancellation’ factor for each scan line, we compute the average absolute field for WSO over all rotations for each scan line (Figure 8) as well as the average absolute field for the corresponding HMI data to get the factor for each scan line as the ratio

$$F = \text{average}(\text{abs}(\text{HMI}))/\text{average}(\text{abs}(\text{WSO})). \quad (1)$$

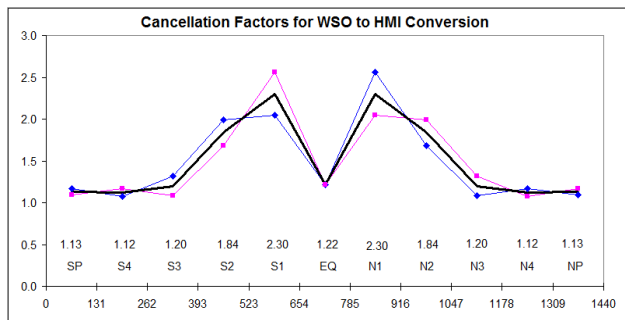


Fig. 8. Variation of the cancellation factor with heliographic latitude (the abscissa is $b = 720 \times (1 + \sin(\text{latitude}))$) as determined for each WSO scan line from the south pole (SP) to the north pole (NP). The blue points show the factor computed as the ratio between absolute field values, eq. (1). The pink points mirror the variation with respect to the equator (EQ), and the heavy black curve shows the adopted symmetric mean variation, also given by the numbers above the scan line designations at the bottom of the Figure.

To a good approximation (better than the data admit) we can

model the factor as an offset plus the sum of two Gaussians (centered on μ South = 544 and μ North = 896) both with standard deviation $\sigma = 70$:

$$F(b) = \frac{251}{\sigma\sqrt{2\pi}} \left(e^{-\frac{(b-544)^2}{2\sigma^2}} + e^{-\frac{(896-b)^2}{2\sigma^2}} \right) + 1.13 \quad (2)$$

where $b \in [0, 1440]$ is the $\sin(\text{latitude})$ bin number (see Figure 8). The scale factor evaluates to 1.42. On the other hand, the factor is rather constant within the polar caps so a formula may be unnecessary overkill.

To see to what degree this makes sense, we apply the so determined cancellation factors to the WSO data and compare to the HMI data as shown in Figure 9. We are most interested in the polar regions where it seems that we can with success convert WSO measurements to the HMI scale.

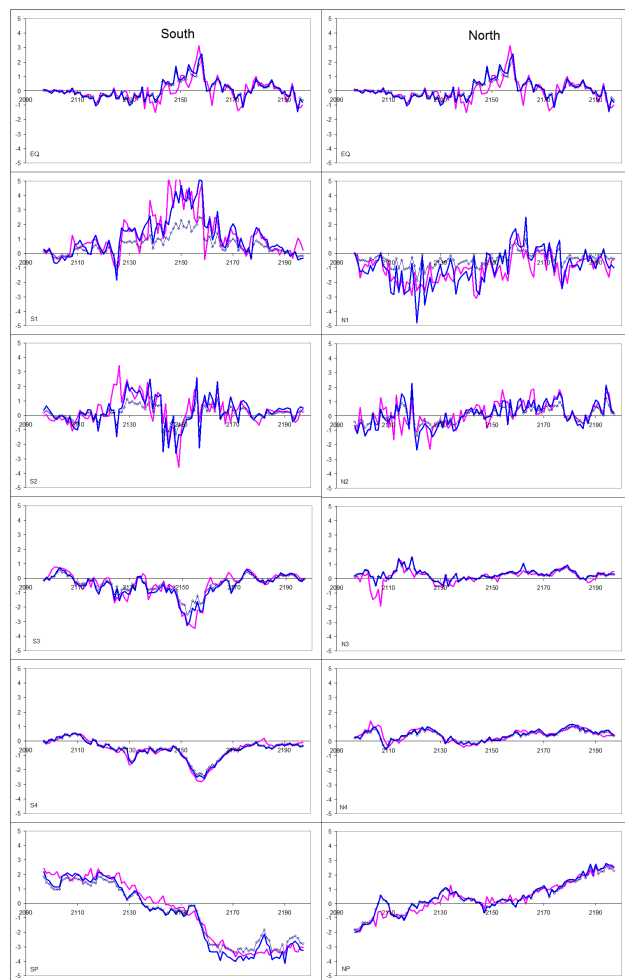


Fig. 9. Variation of the rotation-averaged WSO fields (blue curves) scaled by a latitude-dependent factor (Figure 8) and the corresponding HMI fields (pink curves, since the launch of SDO) averaged over the WSO aperture. The left-hand panel shows the field in the scan lines from the equator to the south pole. The right-hand panel shows the fields in the scan lines up to the north pole. Actual (unscaled) WSO measurement averages are shown by small blue open diamonds. ‘Bumps’ in the four pole-most scan lines move towards the poles at an average 13 m/sec rate, matching the typical rate of meridional circulation.

Keeping a close eye on the most recent HMI super-synoptic maps will show the evolution of the observed polar fields and how they form (Figure 2). This (several narrow ‘streaks’ with both

polarities migrating together) is what the flux transport models should reproduce for us to place any credence in their prediction of the polar fields.

2.3 Possibilities of a Grand Minimum?

The only truly Grand Minimum in the ‘telescope’ era has been the Maunder Minimum (1645-1700). There have since been several ‘centennial’ (but not Grand) minima: the Dalton Minimum (1798-1823), the Gleissberg Minimum (1878-1933), and the still ongoing Eddy Minimum (2009-20??). With Cycle 25 probably being larger than Cycle 24, the chances of a new Grand Minimum unfortunately (as we otherwise would have learned something) seem slim.

References

- Cameron, R. H., Duvall, T. L., Schüssler, M., & Schunker, H. 2018, *A&A*, 609, A56
- Charbonneau, P. 2014, *Annual Review of Astronomy and Astrophysics*, 52, 251
- Clette, F., Svalgaard, L., Vaquero, J. M., & Cliver, E. W. 2014, *Space Sci. Rev.*, 186, 35
- Duvall, Jr., T. L., Scherrer, P. H., Svalgaard, L., & Wilcox, J. M. 1979, *Sol. Phys.*, 61, 233
- Howard, R., Gilman, P. I., & Gilman, P. A. 1984, *ApJ*, 283, 373
- Iijima, H., Hotta, H., Imada, S., Kusano, K., & Shiota, D. 2017, *A&A*, 607, L2
- Jiang, J., Cameron, R. H., Schmitt, D., & Schüssler, M. 2011, *A&A*, 528, A83
- Krause, F. & Raedler, K. H. 1980, *Mean-field magnetohydrodynamics and dynamo theory*
- Leussu, R., Usoskin, I. G., Senthamizh Pavaai, V., et al. 2017, *A&A*, 599, A131
- Lockwood, M., Nevanlinna, H., Vokhmyanin, M., et al. 2014, *Annales Geophysicae*, 32, 367
- Owens, M. J., Cliver, E., McCracken, K. G., et al. 2016, *Journal of Geophysical Research (Space Physics)*, 121, 6048
- Shiota, D. 2018, in *Astrophysics and Space Science Library*, Vol. 449, T. Shimizu et al. (eds.), *First Ten Years of Hinode Solar On-Orbit Observatory*, 173–181
- Steinhilber, F., Abreu, J. A., Beer, J., et al. 2012, *Proceedings of the National Academy of Science*, 109, 5967
- Svalgaard, L. 2014, *Annales Geophysicae*, 32, 633
- Svalgaard, L., Cliver, E. W., & Kamide, Y. 2005, *Geophys. Res. Lett.*, 32, L01104
- Svalgaard, L., Duvall, Jr., T. L., & Scherrer, P. H. 1978, *Sol. Phys.*, 58, 225
- Topka, K., Moore, R. L., Labonte, B. J., & Howard, R. 1980, in *BAAS*, Vol. 12, *Bulletin of the American Astronomical Society*, 893
- Ulrich, R. K. & Boyden, J. E. 2005, *ApJL*, 620, L123